Journal of Physics B: Atomic, Molecular and Optical Physics

PAPER

Correlated electron–nuclear motion during non-adiabatic transitions in LiH and its isotopomers

IOP Publishing Journal of Physics B: Atomic, Molecular and Optical Physics
J. Phys. B: At. Mol. Opt. Phys. **53** (2020) 134001 (11pp) https://doi.org/10.1088/1361-6455/ab84c7

Correlated electron–nuclear motion during non-adiabatic transitions in LiH and its isotopomers

Ksenia G Komarova[1,5], Stephan van den Wildenberg[2], Françoise Remacle[1,2] and R D Levine[1,3,4]

[1] The Fritz Haber Center for Molecular Dynamics and Institute of Chemistry, The Hebrew University of Jerusalem, Jerusalem 91904, Israel
[2] Theoretical Physical Chemistry, UR MolSys B6c, University of Liège, B4000 Liège, Belgium
[3] Department of Molecular and Medical Pharmacology, David Geffen School of Medicine, CA, United States of America
[4] Department of Chemistry and Biochemistry, University of California, Los Angeles, CA 90095, United States of America

E-mail: kgvladi@fh.huji.ac.il

Received 20 December 2019, revised 15 March 2020
Accepted for publication 30 March 2020
Published 2 June 2020

Abstract

Exciting molecules with a short strong few cycle IR pulse triggers coherent electronic–nuclear dynamics on multiple electronic states. This creates a new type of initial state where non-adiabatic transfer takes place between already populated electronic states. We explore this new feature using accurate quantal simulations of the ultrafast laser-induced dissociative dynamics in LiH-LiD-LiT series of isotopomers. In this novel type of initial state the non-adiabatic amplitude exchange between the coupled electronic states strongly depends on isotopic composition. The effective non-adiabatic coupling strength is modulated by two counteracting factors. On one hand, the 1/mass factor makes the non-Born–Oppenheimer coupling weaker for the heavier masses. On the other hand, the transfer is modulated by the momentum coupling of the two non-stationary nuclear wave packets on the two electronic states. The magnitude of this coupling tends to be larger for the heavier isotopes and varies in time as the wave packet dynamics unfold. The correlation in motion of the nuclear wave packets in R- and k-space is then critical. The direction of population transfer changes in time according to the evolution of the coherences built during the short fs excitation. In addition, heavier isotopomers move slower through the non-adiabatic interaction allowing a longer effective duration for the transfer. As a result, an initially very moderate isotope effect in the immediate post excitation population rapidly grows when the wave packets transverse the non-adiabatic coupling region. We compare and contrast with similar time dependent effect of the mass in the non-adiabatic transfer in N_2 where the optically accessible singlet electronic states are all bound and the couplings are quite different.

Keywords: coherent states, non-adiabatic dynamics, isotope effect, ultrafast photochemistry, interference

Supplementary material for this article is available online

(Some figures may appear in colour only in the online journal)

[5] Author to whom any correspondence should be addressed.

1. Introduction

Progress in experimental ultrafast photochemistry [1–4] supplemented and complemented by advances in the theory [5–9] allows the study of the dynamics of a molecule pumped to a coherent superposition of excited electronic states by an ultra short optical pulse. It is not a mixture of states: because of large bandwidth of the pulse in energy each molecule is by itself in a linear combination of several electronic states accessible within this energy range. To each electronic state one can assign a nuclear wave packet, a non-stationary nuclear wave function which can be represented as a coherent superposition of the vibrational eigenstates of that electronic potential. The entire wave packet of correlated electrons and nuclei is initially localized in the Franck–Condon region and shortly after the pulse each nuclear wave packet evolves coherently according to the respective electronic potential. The dynamics of each wave packet reflect the bonding character of the potentials and can be probed via transient absorption [3, 10] or photoionization spectroscopy [6, 8, 11–13].

The coherent superposition of electronic states of the molecule can exhibit unique features during non-adiabatic dynamics. As we discuss here, in particular these features give rise to a strong time dependent isotope effect in the coherent dynamics. The electronic states coupled in a breakdown of the Born–Oppenheimer separation [14] are often of different character. They could be ionic and covalent states [15], which is the case of LiH [16], or Rydberg and valence in N_2 [17]. In the region of their avoided crossing the stationary adiabatic electronic wave functions exchange their character with small variation in the nuclear distance. Such non-adiabatic coupling between electronic states are found to be the rule rather than the exception in the photochemical processes at higher energies [18].

The transfer of the wave packet from one potential to the other is determined by the non-zero coupling terms that are off-diagonal in the electronic index. These terms induce changes in the composition of the initial superposition of states pumped by the pulse. The unique feature of the dynamics originates from the fact that this transfer is modulated by interference of the two nuclear wave packets that make the coupling integral [6, 19–21], analogous to the interference patterns in the Young several-slit experiment. In the coupling region the two nuclear states probe one another as the transfer between them is governed by the relative motion and the stationary phase-difference conditions between the coupled wave packets.

The amplitude exchange between two electronic states is analogous to electronic energy transfer in a collision of two molecules. Except that here the exchange is within one molecule that is coherently in two (or more) different electronic states.

Correlation in the motion of the two 'reactive' nuclear wave packets each along a given adiabatic potential affects the magnitude of transfer between them. For the localized wave packets there is a clear propensity: a large overlap in *R*- and *k*-space is needed and governed by the time-dependent mean values—mean positions and momenta on the coupled states [21]. If the wave packets reach the coupling region at the same time and similar velocities, they will overlap most effectively. The interference pattern seen in the overlap between the coupled wave packets controls the direction of the population exchange [6, 21]. In the case of dynamics on the coupled bound states of N_2, by comparison of different isotopomers we examined the effect of mass on both these aspects, magnitude and direction of transfer. We demonstrated how the history of the dynamics, in particular the nuclear phase accumulated during the motion along the potential, depends on the reduced mass and thereby results in different interference patterns in the population exchange [19]. Similar isotope effect connected to the evolution of the nuclear phases was described by Martin *et al* [22] in the auto-ionization profiles of the pumped coherent wave packets in H_2/D_2.

In the present work we examine the dynamics on the coupled dissociative potentials of LiH, figure 1(a), and contrast it with the case of N_2 where longer time dynamics unfolds on the bound singlet potentials. For N_2 there will be several recurrences of the wave packets in the coupling region, hence the isotope effect persists in time. There is no recurrence on the dissociative electronic states of LiH. Therefore the non-adiabatic dynamics is not as persistent as that observed in N_2. So the correlation in motion on the two repulsive states becomes critical for efficient population transfer. LiH serves as a rough introduction to the dynamics for polyatomic molecules with many vibrational degrees of freedom, where the recurrence of the wave packets is less probable. We report that as in N_2 also in the case of LiH there is a strong time-dependent isotope effect originating from constructive overlap of the coupled wave packets. In addition and importantly, in LiH the interference affects the asymptotic yield into the different exit channels.

The initial coherent state in LiH has qualitative differences compared to the UV-excited coherent state of N_2. First, the strong IR pump pulse used induces multiphoton transitions toward a large band of excited electronic states and enables transfer to the ground electronic state of the cation and its photoionization continuum. Second, as the excited states are of alternating polarity large electronic transition dipoles between them induce very rapid population exchange during the strong IR-pulse. Our results show that even in the presence of such an extensive electronic reorganization during the field, the initial isotope effect on the population at the very early times is quite moderate. This supports the idea that initial coherences built by the pulse are similar for different isotopomers and enables us to discern the effect of the nuclear motion and nuclear mass on the non-adiabatic dynamics after the pulse.

Accurate *ab initio* quantum chemical computations [23–27] of the adiabatic state potentials for the excited states of LiH are reported in the literature. For the response to the strong pulse that we aim to simulate electronic states all the way to ionization are accessed. We use the state-averaged (SA) CAS–SCF level of theory described in reference [23] for computing the potential, dipole and non-adiabatic coupling curves of a band of 19 states of the neutral converging to the ionization limit and the four states of the cation as a function of the internuclear distance up to 20 Å (a table of the potentials is provided in a supplementary data file, which can be found

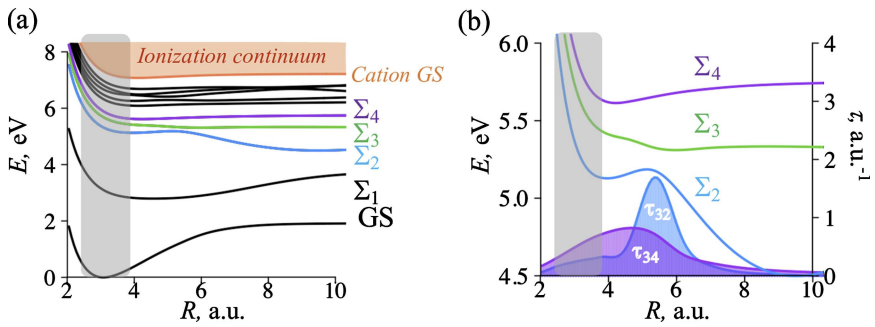

Figure 1. (a) Potentials of the ground (GS) and of the 9 lowest excited singlet Σ electronic states of the neutral LiH and the Σ ground state of the cation involved in the field-induced dynamics, adapted from [23]. The potentials of the 3 excited states: Σ_2, Σ_3 and Σ_4 are strongly coupled at the exit of the FC region and highlighted with color. (b) Potentials and non-adiabatic couplings τ between the strongly coupled states. The Franck–Condon region of the ground state is shown as a grey shaded area. As the bond is stretched, the ionic character of the GS is transferred to higher excited electronic states through strong non-adiabatic coupling.

online at http://stacks.iop.org/JPhysB/53/134001/mmedia). While not reaching the accuracy required to compare with high resolution spectroscopic results [24], the SA–CASSCF level used here allows for implementing quantum dynamical simulations taking into account non-adiabatic coupling, photo excitation for a band of 10 $^1\Sigma^+$ states in the neutral coupled to the GS of the cation by photoionization.

We focus on states of $^1\Sigma^+$ symmetry and we refer to them as Σ states for brevity (figure 1). The potentials of the three states Σ_2, Σ_3 and Σ_4 ($3^1\Sigma^+$, $4^1\Sigma^+$ and $5^1\Sigma^+$ in spectroscopic notation) [23] that are important for the non-adiabatic dynamics that we discuss agree quite closely with those computed by Gadea and Leininger [24]. The strong non-adiabatic couplings, τ_{23} between the $\Sigma_2 - \Sigma_3$ states and τ_{34} between $\Sigma_3 - \Sigma_4$ repulsive excited states of LiH are localized in immediate proximity to the Franck–Condon region, figure 1(b). This allows examining the non-adiabatic dynamics between the pumped wave packets on these electronic states after the pulse is turned off, within the first 50–100 fs [23]. The localization of the coupling facilitates the examination of dynamical effects, such as time-dependent position, momentum and phase of the non-stationary wave packet. A wave packet picture is a suggestive analogue to the Landau–Zener model for the adiabatic/diabatic types of transfer [28]. There is however one difference with the classical trajectory model of Zener [29]: in the present study both electronic states are initially populated.

Further on the way to dissociation there is a second coupling region, see figure S1 in the supplementary information (SI). The transfer is not efficient in this region because the coupled wave packets do not reach it at the same time. So we focus on the first region of coupling at shorter internuclear distances which affects the population dynamics at earlier times.

The paper is organized as follows. In the next section essential background information is outlined. Then the computational details for the field-induced quantum dynamics simulations on the grid are reviewed. In this section we describe also the details about the analysis of the wave packets and the coupling integrals computed on the grid using the expansion (1) in either R- or k-space. In section 4 the results for the isotope effect in the population dynamics are shown. The origin of the role of the mass is examined using simple approximate analytical formulas for the coupling integrals in comparison with the accurate numerical results. The connection between the coupling integral and the coherence in the k-space is discussed. Finally the condition on the stationary nuclear phase difference for the efficient non-adiabatic transfer is analyzed.

2. Background

We analyze the dynamics in different isotopomers to extract parameters of the coupled electronic–nuclear motion that have a major effect on the non-adiabatic transfer and the yield of products. The electronic–nuclear motion consists of the coherent motion of two nuclear wave packets each along a given electronic state and the interference between them. The motion can be characterized by the properties of the wave packets such as the mean position and the mean momentum and higher moments. Here we will use the first and second moments of the exact wave function to generate a Taylor expansion of the wave function. This will allow a direct interpretation of the isotope effect in the exact computation.

The interference requires examination of the phases of the two coupled wave packets. There are two contributions to the phase difference. One is the energy difference, $\Omega_{21}t = \left(\langle E_2\rangle - \langle E_1\rangle\right)t$, where the averaging is over the nuclear wave packet on the particular electronic state [21] referred to by the subscript. Ω_{21} is the 'beating frequency' of the coherence between the two nuclear wave packets. Another component of the phase difference comes purely from the nuclear dynamics as it is driven by the mean momentum of the respective nuclear wave packet. For an effective transfer this phase-difference needs to be stationary which results in a large non-adiabatic transfer between the electronic states. We found this in N_2 and we will show that it also is true for the case of the dynamics in LiH.

We use the parameterization of the motion of a nuclear wave packet on a given electronic state in a quadratic potential in the form proposed by Heller [30, 31]. The wave function is defined by a Taylor series of $\ln\chi$ around the mean value of the 1D internuclear distance, $\langle R(t)\rangle$:

$$\chi(t) \approx \exp\left[i\alpha\cdot\left(R-\langle R\rangle\right)^2 + i\langle P\rangle\left(R-\langle R\rangle\right) + i\gamma\right] \quad (1)$$

here $\{\alpha, \gamma, \langle R\rangle, \langle P\rangle\}$—are time-dependent parameters: complex width, phase, and mean values of the coordinate $\langle R\rangle$ and momentum $\langle P\rangle$. Heller identified the nuclear phase $\gamma(t)$as a coefficient of a zeroth order term $\left(R - \langle R\rangle\right)^0$. By writing a Taylor expansion for the potential also up to the second order around the mean $\langle R(t)\rangle$ in the time-dependent Schrödinger equation, and collecting all the coefficients in front of the same powers of $\left(R - \langle R\rangle\right)$, Heller derived the time evolution of this phase as:

$$\frac{d\gamma}{\mathrm{d}t} = \langle P\rangle \frac{dR}{\mathrm{d}t} = \langle P\rangle^2/m. \tag{2}$$

One can see that $\gamma(t)$ is determined by the mean momentum $\langle P\rangle$, and is also explicitly dependent on the reduced mass, m. This phase enters as a zeroth-moment term in the Taylor expansion of the wave function. For anharmonic or repulsive potentials higher powers of the Taylor expansion need to be included. However, this will not affect the coefficient of the zeroth moment. We can therefore use equations (1) and (2) to describe the isotope effect for the repulsive potentials of LiH.

Finally, it is important to note that we follow the isotope effect in the transfer of population between specific electronic states, hence it depends on the chosen basis representation for the electronic subspace. The strong effect of mass on the population exchange in N_2 was initially described in the diabatic representation. For the electronic states in this representation the kinetic energy is diagonal and the coupling between the electronic potentials comes from the electronic Hamiltonian. Therefore the so-called diabatic coupling $V_{12}(R)$ is not mass-dependent, and the coupling integral can be written in the Condon approximation simply as a product of the effective coupling at the mean position and the overlap integral: $V_{12}(\bar{R}(t)) \cdot \langle \chi_1(t,R)|\, \chi_2(t,R)\rangle$. In this case the direct connection between the coupling integral and the coherence, or interference, between the wave packets on the coupled electronic states is explicitly evident. In a recent paper [32], we have shown that the isotope effect is also present if one uses an adiabatic electronic basis to describe the dynamics in N_2. In the case of the adiabatic representation, which we use also in the present study, the coupling integral, which originates from the off diagonal kinetic energy non Born–Oppenheimer terms [14, 33], $(1/m) \cdot \langle \chi_1|\, \tau_{12}\hat{P}\, |\chi_2\rangle$, is (i) explicitly dependent on mass and (ii) includes the momentum operator that acts on the nuclear wave packet. To clarify the connection to the coherence, we discuss the components of this integral in the k-space, where the integrand of $\langle \chi_1|\, \hat{P}\, |\chi_2\rangle$ is a simple product: $k \cdot \tilde{\chi}_1^*(k,t)\tilde{\chi}_2(k,t)$. The two components of the phases that are discussed above are not R-dependent and therefore will have a similar role also in the coherence expressed in k-space.

3. Computational details

3.1. Quantum dynamics on the grid

In what follows we mention only the essential steps in the simulation, while for further details about the quantum chemistry of LiH and the photoionization dynamics we refer to [23]. In section S2 of the SI we provide technical details about the dynamical computations.

Quantum dynamics of a non-rotating LiH molecule is computed by numerically integrating the time-dependent Schrödinger equation on a one dimensional grid of Li–H internuclear distance, R [34]. The Cartesian molecular frame is attached to the center of mass, and the molecule is oriented along the z axis with $z_{\mathrm{Li}} > 0$, $R = z_{\mathrm{Li}} - z_{\mathrm{H}}$, see figure S1 in the SI. For each grid point the Hamiltonian matrix elements are defined for the two orthogonal subspaces of 10 adiabatic neutral and 1 cationic electronic states of LiH. The neutral electronic states are coupled together both by the interaction with the electric field associated with the pulse, in the dipole approximation, and by the nuclear motion, through non-adiabatic coupling. The neutral and cation subspaces are coupled by the interaction with the electric field through the photoionization coupling elements that were computed using the method described in reference [23].

The strong IR one-cycle pulse is treated semi-classically via the dipole approximation with the time-dependent Gaussian profile of the electric field polarized along the LiH molecular axis:

$$E(t) = |E_{\max}| \exp\left(-\left(t - t_p\right)^2/2{\sigma_t}^2\right) \times \left(\cos(\omega t) - \frac{\left(t - t_p\right)}{\omega\sigma_t^2}\sin(\omega t)\right) \tag{3}$$

here the carrier wavelength is set to 720 nm ($\omega = 1.17$ eV), a peak intensity of $1.14 \cdot 10^{13}$ W cm^{-2} (field strength $|E_{\max}| = 0.017$ a.u.) and a FWHM of 3.5 fs ($\sigma_t = 1.5$ fs). The FWHM in energy of the pulse is about 1 eV, so that the variance of the Gaussian envelope of the pulse in the frequency domain is $\sigma_\omega = 0.44$ eV. The carrier-envelope phase is taken to be zero, which corresponds to the electric field at its maximum pointing towards the Li-nucleus.

The LiH molecules with their high permanent dipole moment are assumed to be oriented so that the laboratory frame coincide with the molecular frame, therefore only the states of Σ symmetry are accessed by the pulse. For symmetry breaking by the field see discussion in [35]. This will allow non-adiabatic coupling between the states of Π symmetry as well. We focus here on the very short timescale of the dynamics, first 50–100 fs, and therefore no effects of rotation are taken into account. The experimental possibilities to align molecules using their dipole moments are discussed in [36] with attention also being given to ultrashort laser pulses in [37].

To describe the isotope effect in the population dynamics we perform a separate calculation of the field-induced quantum dynamics for each given LiH–LiD–LiT reduced mass, 1617.95/2873.10/3872.68 a.u. respectively. The change in the reduced mass of the system in the adiabatic picture has no effect on the electronic Hamiltonian. The potentials, dipoles and derivative coupling terms between the electronic states $|\psi_j\rangle$and$|\psi_k\rangle$, $\tau_{jk} = \langle\psi_j|\partial\psi_k/\partial R\rangle$, are taken to be the same for different isotopomers. In the molecular Hamiltonian the non-adiabatic couplings, NACs, are obtained by multiplying the coupling τ_{jk} by the momentum operator and dividing by the

mass of the respective isotopomer:

$$NAC_{jk} \equiv -(1/m_{LiX}) \cdot \tau_{jk}(R) \frac{\partial}{\partial R}. \quad (4)$$

The change of mass therefore contributes both to the dynamics along the single adiabatic potential through the kinetic energy term and to the non-adiabatic coupling between pairs of the electronic states.

The terms of the electronic Hamiltonian: potentials, permanent and transition dipoles, and non-adiabatic couplings are computed at each internuclear distance via the state-averaged CAS SCF using 6-311++G (3df, 3dp) Gaussian basis set augmented by 2S, 3P and 3D Rydberg orbitals centered on the H atom [23]. Large active space of 4 electrons and 20 molecular orbitals is crucial in properly describing the convergence of the 10 Σ electronic states of the neutral toward the 1 Σ state of the cation. All the quantum chemical computations are performed using the MOLPRO package [38–42].

The population on each grid point on each electronic state $|\psi_{kg}\rangle$ for the propagated wave function $\Psi(t)$ is used to define the population n_k on electronic state k as:

$$n_k = \sum_g \langle \Psi(t)|\psi_{kg}\rangle \langle \psi_{kg}|\Psi(t)\rangle = \sum_g |c_{kg}|^2 \quad (5)$$

where $|c_{kg}|^2$ is population of the state at a grid point g and sum runs over N-grid points. The wave functions in the k-space are computed using the standard fast Fourier transform routines [43, 44].

3.2. Analysis of the dynamics using a Taylor series expansion

We define a model wave packet $\chi_k(t, R)$ on each electronic state $|\psi_k\rangle$ as discussed in equation (1) by multiplying it by its time dependent amplitude $c_k(t)$:

$$\chi_k(t, R) = c_k(t) \exp\left(i\alpha_k(R - R_k)^2 + iP_k(R - R_k) + i\gamma_k\right). \quad (6)$$

The parameters R_k etc are calculated for the exact wave packets $\Psi_k(R, t)$ propagated on the grid at each time step of the dynamics, for example: $R_k = \langle \Psi_k(R, t)| \hat{R} |\Psi_k(R, t)\rangle$. The values of real and imaginary parts of the complex width $\alpha_k(t)$ are defined from the given dispersion in the probability distribution in R and k-space, σ_R^2 and σ_P^2 (see also section S1 of the SI):

$$\mathrm{Im}(\alpha_k) = \frac{1}{4\sigma_R^2} \quad \mathrm{Re}(\alpha_k) = \frac{\sqrt{4\sigma_R^2\sigma_P^2 - 1}}{4\sigma_R^2}. \quad (7)$$

We define the zeroth order term $c_k(t) \cdot \exp[i\gamma_k(t)]$ in accord with the Taylor expansion using the value of the exact wave packet at the grid point nearest to the mean $R_k(t)$:

$$c_k(t) \cdot \exp[i\gamma_k(t)] = \Psi_k(R, t)|_{R=R_k(t)}. \quad (8)$$

With this, the analytical expression is complete and one can trace the effect of mass on specific nuclear observables. Such an approximation can capture the main features of the localized non-stationary nuclear wave function that evolves on a smooth potential. As the dynamics unfolds the wave packet splits into several branches and the single Gaussian toy model is no longer accurate for longer times.

4. Results and discussion

4.1. Field-induced dynamics and the isotope effect

Population dynamics in the LiH–LiD–LiT molecules during and after the pulse are shown in figure 2 for the important excited states. Populations in the full 11 states basis can be found in figure S2 of the SI. The populations at each time step are evaluated for the exact wave packets using equation (5).

For all three isotopomers the population during the pulse is about the same, with substantial ionization of about 25% and 8.5% of the population in the excited electronic states, figure 2(a). After the field, non-adiabatic coupling between the Σ_3 and Σ_4 states induces extensive population exchange already within 15–20 fs, figure 2(b). The isotope effect in the transfer for this pair of states is weak at early times of the population exchange but rapidly increases at about 30–40 fs, figure 2(b). Similarly, in the coupling of Σ_3 to Σ_2: strong effect of mass is seen only at later times of the transfer at 40–45 fs, figure 2(c). The states are dissociative so the mass-sensitive transient dynamics alters the yield in each electronic state in the exit region, shown for example in Σ_4 state around 45 fs in figure 2(b).

We begin the analysis of the isotope effect by examining the rate of change of the populations in the exact computation. We estimate the rate as a derivative of the population with respect to time using the simplest 3-point finite difference approximation. The calculated rate for the Σ_3 state is shown in figure 3(a). The rate of transfer exhibits several oscillations which reflect the beating of the coherence between the coupled states as we will discuss in the section 4.3. At the first peak around 20 fs the rate is almost twice as large for the LiH compared to LiD/LiT. At the next few peaks the magnitude of the transfer alternates and the heavier isotopomers exhibit higher rates. Post this the rate decreases with time most rapidly for the lightest isotope. The sign of the rate determines the direction of transfer and it changes sequentially, 'depletion–acquiring–depletion' for the well-resolved three peaks in the heavier species. As emphasized in section 2, the population transfer is induced by the mass dependent non-adiabatic coupling integral $(1/m) \cdot \langle \chi_1| \tau_{12} \hat{P} |\chi_2\rangle$. This integral is a product of two factors that act in an opposite way when the reduced mass of the molecule is changing. It is clear from this equation that the $1/m$ factor tends to reduce the rate of transfer as the mass of the isotope rises. To eliminate the dependence of the coupling integral on this factor, we scale the computed rate of population transfer by the isotopic mass, leading to figure 3(b). As the influence of the $1/m$ factor is removed, we can see that the remaining coupling integral is clearly dependent on the isotopic mass and is higher for heavier masses.

4.2. Condon approximation for the coupling integral

To understand the origin of the isotopic effect on the non-adiabatic rate of transfer we build an analytical model. Using

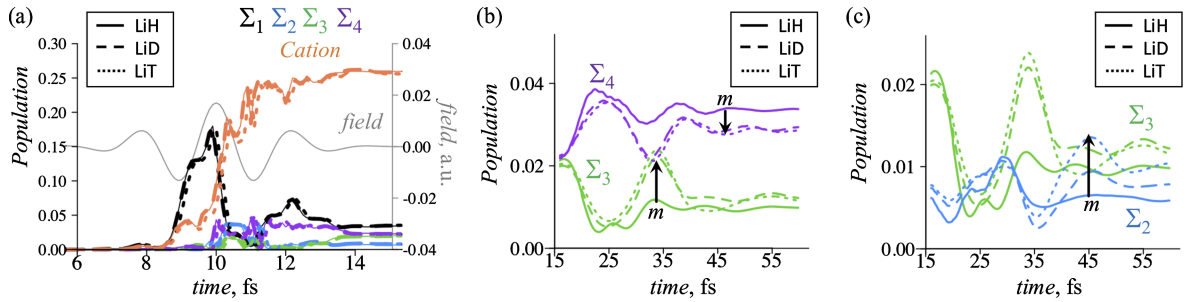

Figure 2. Isotope effect in the quantal accurate non-adiabatic dynamics. (a) Population dynamics during the field and (b) and (c) dynamics after the field in the (b) $\Sigma_3 \Leftrightarrow \Sigma_4$ and (c) $\Sigma_3 \Leftrightarrow \Sigma_2$ coupled channels. Shown are the populations of the Σ_1 (black), Σ_2 (blue), Σ_3 (green), Σ_4 (purple) excited states and the ground state of the cation (orange) for LiH (solid lines), LiD (dashed lines) and LiT (dotted lines). The profile of the pulse is shown as a grey line in panel (a). Initially the population is not sensitive to the reduced mass, m. For the $\Sigma_3 \Leftrightarrow \Sigma_4$ case the isotope effect increases significantly after 30 fs of the dynamics, reaching in Σ_3 almost 50% of the overall population (shown with a black arrow). The effect of mass on the $\Sigma_3 \Leftrightarrow \Sigma_2$ population exchange is maximal around 45 fs of the dynamics. The transient exchange affects the asymptotic yield for the population in different states, which is also sensitive to the mass as seen at longer times in both panels (b) and (c).

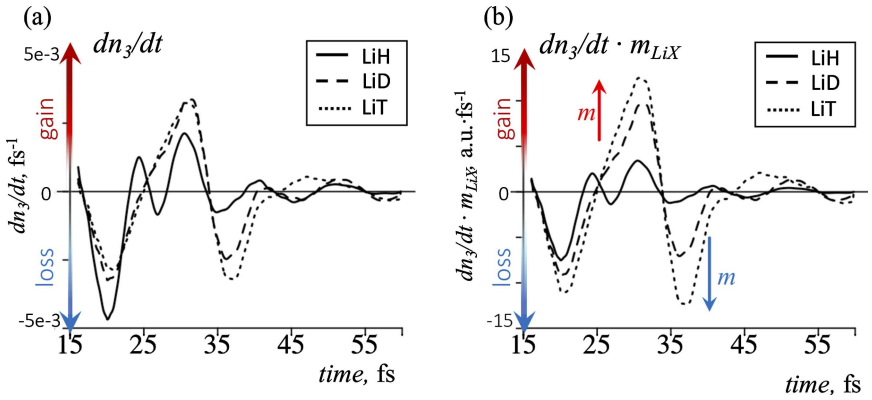

Figure 3. Isotope effect in the rate of transfer. (a) The rate of population transfer, dn_3/dt, in the Σ_3 state during the transient non-adiabatic dynamics in LiH (solid lines), LiD (dashed lines) and LiT (dotted lines). (b) The rate of transfer scaled by the reduced mass m_{LiX} of the respective molecule. Negative values of the rate correspond to loss in the Σ_3 population and positive values to gain in the population. Note the ratio between the isotopomer reduced mass and the mass of LiH is 1.8 and 2.4 for LiD and LiT. Larger gain/loss in the population for the heavier masses at 30 fs and 37 fs is highlighted with red/blue arrows, respectively.

the Liouville–von Neuman quantal equations of motion for the population in the adiabatic basis of electronic states (see detailed derivation in section S2 of the SI) we compute a non-adiabatic rate of transfer that has a simple analytical expression. We consider the dynamics after the pulse and therefore we can limit our basis only to the set of coupled Σ_2–Σ_4 states. To simplify the analysis we allow only the coupling between the neighbouring pairs of states $\{\tau_{32} : \Sigma_3 \Leftrightarrow \Sigma_2\}$ and $\{\tau_{34} : \Sigma_3 \Leftrightarrow \Sigma_4\}$. In this basis of three coupled electronic states we here focus on the equation of motion for the population on the Σ_3 state:

$$\frac{dn_3}{\mathrm{d}t} = -\frac{2}{m}\mathrm{Re}\left[\langle 3|\,\tau_{32}\hat{P}\,|2\rangle\right] - \frac{2}{m}\mathrm{Re}\left[\langle 3|\,\tau_{34}\hat{P}\,|4\rangle\right]. \qquad (9)$$

The coupling integrals above include integration over the nuclear coordinate:

$$\langle 3|\,\tau_{32}\hat{P}\,|2\rangle = -i\int \Psi_3^*(R,t)\tau_{32}(R)\frac{\partial\Psi_2(R,t)}{\partial R}dR \qquad (10)$$

where $\Psi_k(R,t)$ denotes the exact wave packet on the electronic state Σ_k propagated on the grid accounting for the full basis of 10 electronic states.

We further simplify the integral by assuming that the two coupled wave packets are localized close enough for a Condon approximation to be valid:

$$\langle 3|\,\tau_{32}\hat{P}\,|2\rangle \approx \tau_{32}(\bar{R})\cdot\langle 3|\,\hat{P}\,|2\rangle \qquad (11)$$

here $\tau_{kn}(\bar{R})$ is the effective value of the non-adiabatic coupling between the pair of state k and n taken at the distance R averaged between the mean values R_k and R_n:$\bar{R} = [R_k(t) + R_n(t)]/2$.

Comparison between the approximate population dynamics determined using equations (9) and (11) and the full 10-state exact results for LiH and LiT isotopomers is presented in figure 4. Good correspondence in the isotope effect between the exact numerical and analytical populations justifies the assumptions made in deriving equations (9) and (11). This allows us in the next section to relate the isotope effect to the two components of equation (11).

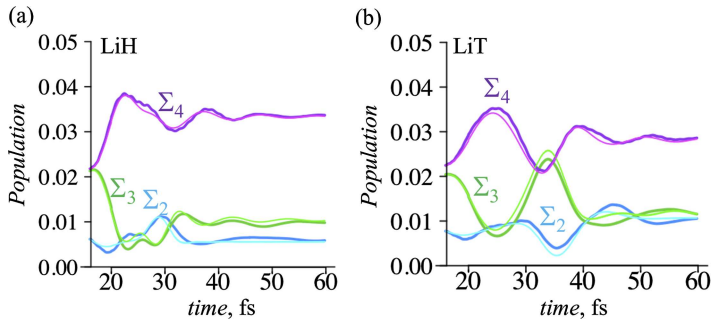

Figure 4. Population dynamics for the coupled Σ_2 (blue), Σ_3 (green), Σ_4 (purple) electronic states in LiH (a) and LiT (b). The curves with a brighter shade of the color represent the analytical 3-state population dynamics computed within the Condon approximation, equations (9) and (11). The curves in deeper colors show the results of the full quantum dynamics simulation for the 10 coupled electronic states of the neutral system.

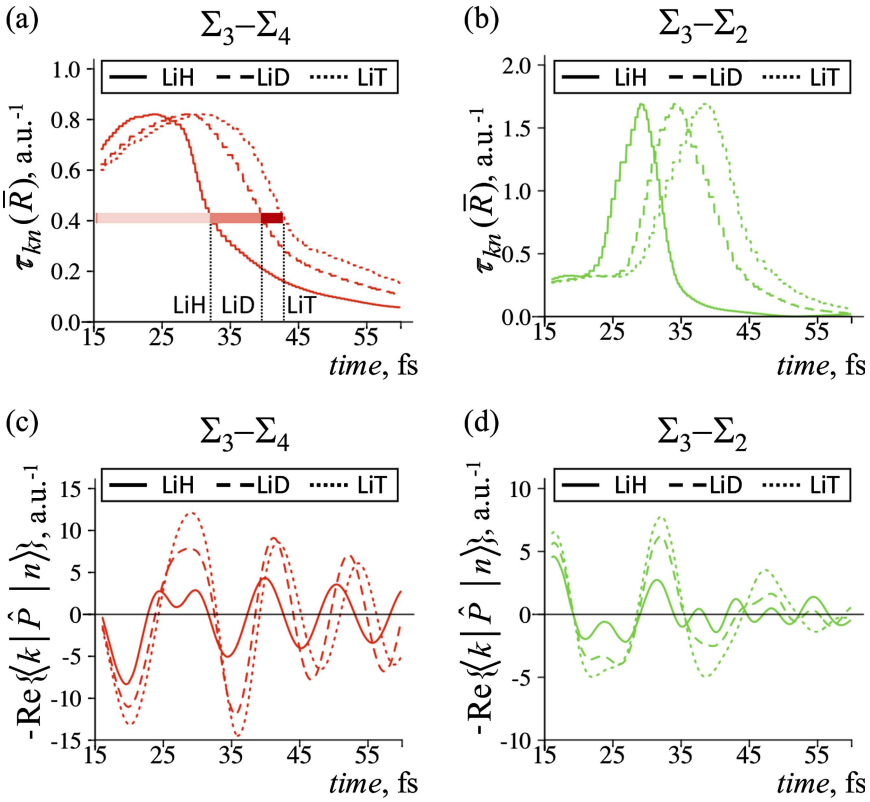

Figure 5. Components of the two coupling terms in equation (11) for the population transfer of the Σ_3 state for the $\{\Sigma_3 \Leftrightarrow \Sigma_4\}$ and $\{\Sigma_3 \Leftrightarrow \Sigma_2\}$ coupling channels, shown in red and green colors, respectively, in LiH (solid lines), LiD (dashed lines) and LiT (dotted lines). (a) and (b) Non-adiabatic coupling at the mean R averaged over the two electronic states; (c) and (d) the real part of the momentum integral. Faster exit from the coupling region for the lighter isotopomer can be clearly noted in both coupling channels, highlighted in the width of the effective coupling in panel (a). The coupling $\tau_{kn}\left(\bar{R}\right)$ acts to quench the oscillations of the $\langle k|\,\hat{P}\,|n\rangle$ integral.

4.3. Coupling integral and the coherence

We discuss dynamics in the $\Sigma_3 \Leftrightarrow \Sigma_4$ and $\Sigma_3 \Leftrightarrow \Sigma_2$ coupling channels. Comparison between the individual contribution from each channel to the overall rate of transfer, equation (9), is shown in figure S3 in the SI. At the first peak in the rate of transfer, figure 3, the major depletion of the Σ_3 population is due to its coupling to the Σ_4 state. After 25 fs of the dynamics, as the coherent wave packet moves closer to the $\Sigma_3 \Leftrightarrow \Sigma_2$ non-adiabatic coupling region population exchange with the Σ_2 state starts to be significant.

Components of the coupling integrals, equation (11), for the two channels are presented in figure 5. The top row shows evolution in time of the magnitude of the effective coupling, $\tau_{kn}(\bar{R})$, while the bottom panels show the real part of the momentum coupling integral $\langle k|\,\hat{P}\,|n\rangle$. By definition $\tau_{kn}(\bar{R})$ is related to the change of the mean $\langle R\rangle$ on the coupled states, see figure S4 in the SI. As a function of time $\tau_{kn}(\bar{R})$ has a maximum at a longer time for the heavier isotopes. The duration of the coupling, the width of the effective coupling in time, is also increasing as the wave packets are transversing

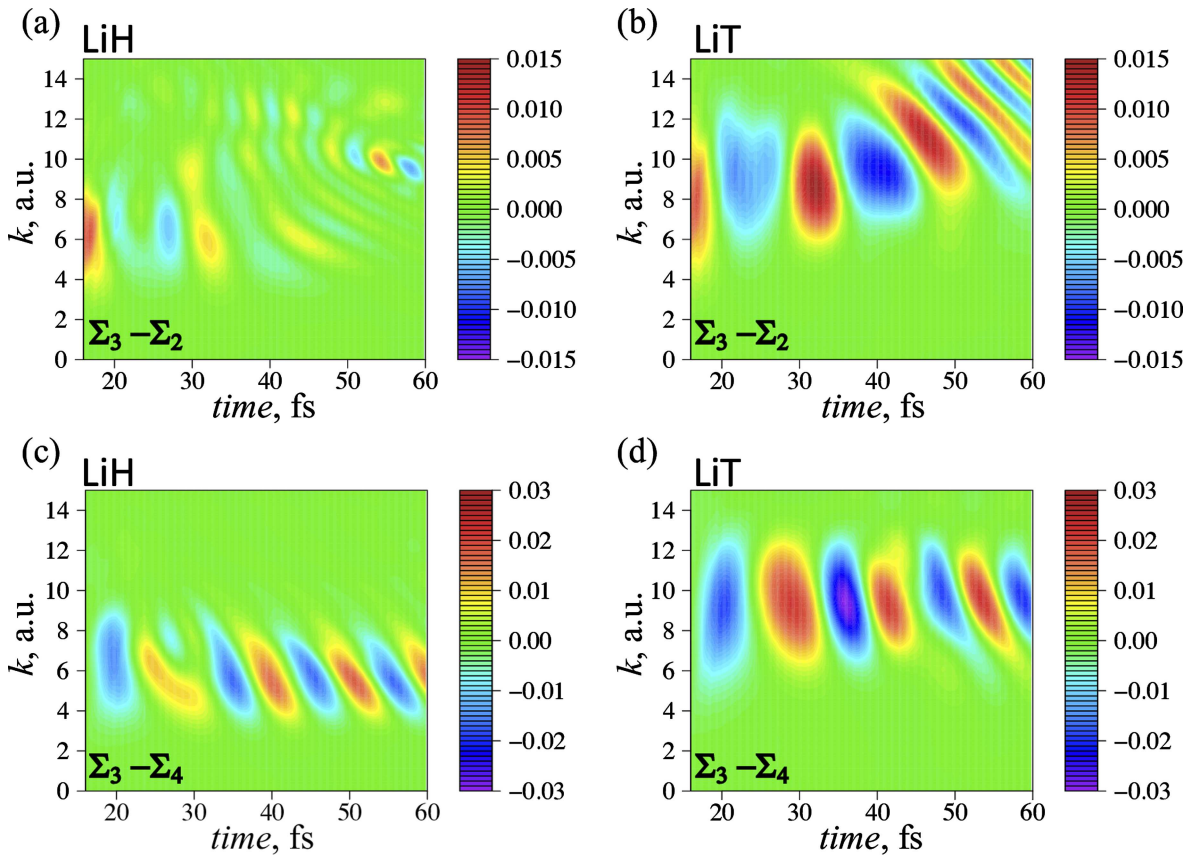

Figure 6. A heat map representation, for LiH and LiT of the integrand of $-\mathrm{Re}\left[\langle k|\,\hat{P}\,|n\rangle\right]$, contributing to equations (9) and (11), between the Σ_3 and Σ_2 (a) and (b) and the Σ_3 and Σ_4 (c) and (d) states in momentum space. Shown as a function of momentum, k, vs. time.

the interaction region more slowly, see the highlighted region in figure 5(a). The efficiency of the non-adiabatic coupling therefore becomes larger.

The interference between the wave packets enters through the momentum integral. This can be seen by comparison of the gain–loss dynamics in the rate of transfer, figure 3, and the oscillatory behavior in the momentum integral, figures 5(c) and (d). The magnitude in the momentum integral is very much affected by the reduced mass. To show this explicitly, figure 6 exhibits the integrand as a heat map in momentum space where the action of the momentum operator is just a multiplication of the coherence by k. The maps for LiD are given in figure S5 of the SI. Note the larger momentum for the heavier mass and the higher width for both coupling channels. In the case of $\Sigma_3 \Leftrightarrow \Sigma_2$ channel, the oscillation of the coherence in LiH, figure 6(a), are clearly different from the two other isotopomers. We next examine the relevant parameters for oscillations in the interference.

4.4. Stationary phase difference during the non-adiabatic transfer

We discuss the non-adiabatic transient exchange between two electronic states that are both populated at the onset of the coupling. As shown in figure 6 and earlier this is determined by the overlap of the two wave packets. This is unlike the Landau–Zener model where only one state is initially populated, see [28, 29] in particular. To estimate the overlap of the two wave packets we use the expansion shown in equation (6). Comparison between the exact heat maps of the integrand of $\langle k|\,\hat{P}\,|n\rangle$, figure 6, and maps obtained using the Taylor expansion are given in figure S6 of the SI. These show that the approximation using from the zeroth to the second moment is accurate in the time range where the isotope effect is strong.

Using the Taylor expansion the overlap of the two wave packets can be written as:

$$\langle\chi_k|\chi_n\rangle = \Xi_{kn}\Phi_{kn}\,\exp\left(-\eta_{kn}(P_k - P_n)^2 - \xi_{kn}(R_k - R_n)^2\right) \tag{12}$$

$$\Phi_{kn} = c_k^* c_n\,\exp\left(i\Delta\gamma_{kn}\right) \tag{13}$$

here R_i and P_i are the mean values of the coordinate and momentum in the electronic state i. The other parameters in equation can be found in section 3 of the SI. This equation shows that large values of the overlap require the two packets to be localized in the same place and to have a comparable momenta. The magnitude of the momentum coupling integral, $\langle\chi_k|\,\hat{P}\,|\chi_n\rangle$, in the Condon limit $R_k = R_n \equiv \bar{R}$ and $P_k = P_n \equiv \bar{P}$ has direct relation to the overlap:

$$\langle\chi_k|\,\hat{P}\,|\chi_n\rangle = \bar{P}\,\langle\chi_k|\chi_n\rangle\,. \tag{14}$$

Analytical formula for the $\langle\chi_k|\,P\,|\chi_n\rangle$ integral in general case is given in section 3 of the SI. Equation (14) shows that the magnitude of the transfer scales with the value of the mean momentum. This explains the larger values of the integral for

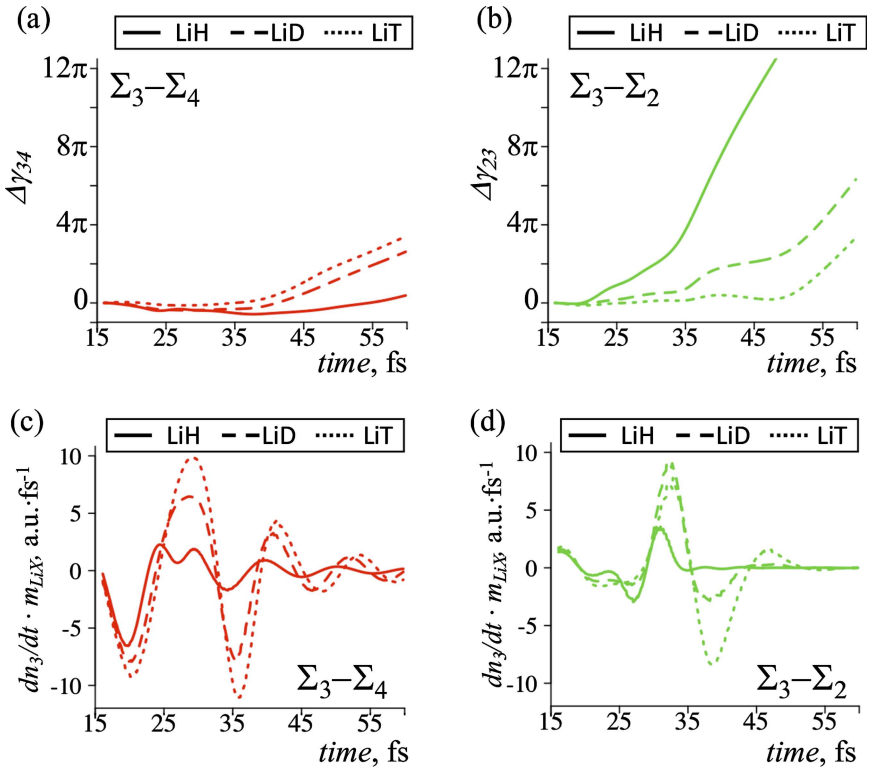

Figure 7. The phase-difference, $\Delta\gamma(t)$, (a) and (b) versus the magnitude of the rate of transfer (c) and (d) in LiH (solid lines), LiD (dashed lines) and LiT (dotted lines) for the $\{\Sigma_3 \Leftrightarrow \Sigma_4\}$ (a) and (c) and $\{\Sigma_3 \Leftrightarrow \Sigma_2\}$ (b) and (d) coupling channels, shown in red and green colors, respectively.

the heavier isotopes. Divided by the reduced mass in the final form for the rate of transfer, equation (9), it can be regarded as a mean velocity, $d\langle R\rangle/\mathrm{d}t \approx \langle P\rangle/m$ of localized wave packets. From the exact dynamical computations of the $\langle R\rangle$ vs time, shown in figure S3 in the SI, one can see that the velocity is smaller for the heavier isotopomers. This approximate treatment explains the lower rates of transfer for the heavier masses at the early time dynamics. At later times, faster exit from the coupling region for the lighter isotopomer, see $\tau_{kn}(\bar{R})$ dynamics in figures 5(a) and (b), results in less effective transfer.

Another important term that governs the overlap in the Condon limit is the constant in R factor Φ_{kn}, equation (13). This term changes rapidly with time for two reasons. One is the phase factor $\Delta\gamma_{kn} = \gamma_k - \gamma_n$ see equation (2) and figure S7 in the SI for the evolution of the phases of the wave packet on each electronic state. The other component of this factor: $c_k^* c_n \approx \exp(i\Omega_{kn}t)$, oscillates with a frequency related to the gap between the two electronic states, figure S8 in the SI. For an effective transfer these two components should interfere constructively with a beating at one dominant frequency, here Ω_{kn}. So in both N_2 and LiH and its isotopomers we find that the difference in phase between the two wave packets, $\Delta\gamma(t)$, needs to be essentially stationary in the time interval of a large rate, see figure 7.

As can be seen in figure 7, in the time frame when the effective coupling, $\tau_{kn}(\bar{R}(t))$, is large in almost all cases the $\Delta\gamma(t)$ is stationary. Exception is the case of LiH during the $\Sigma_2 \Leftrightarrow \Sigma_3$ transfer. In the time range of large $\tau_{kn}(\bar{R}(t))$, 23–35 fs, the phase difference $\Delta\gamma(t)$ in LiH is growing rapidly, figure 7(b). Change of the phase difference from 0 to 2π results in faster oscillations in the integral and lower rate of transfer compare to the other isotopomers.

The condition for the phase difference to be stationary can be written as a propensity rule: $\left(P_k^2 - P_n^2\right)/m \approx 0$. In such a form the effective transfer is large when the difference in the momenta on the coupled states, $P_k^2 - P_n^2$, is small compare to the reduced mass of the system. This is reminescent to the process of energy transfer during molecular collision [28].

In view of the condition on the momenta the effect of mass is different for the two coupling channels considered. In the case of $\Sigma_3 \Leftrightarrow \Sigma_4$ channel in the region of the avoided crossing their potentials are quite similar in shape, see figure 1(b). This provides similar effect of mass on the mean momenta for their wave packets and weak isotope effect on the difference $P_3^2 - P_4^2$ in the time frame of interest, see figure S9 in the SI. In contrast, the Σ_2 potential has a steeper slope in the Franck–Condon region. This results in faster evolution of the momentum on the Σ_2 state, compare figure S9 (a) and (b) in the SI in the early time range 15–20 fs. Close matching of the momenta on the coupled states occurs only for the heavier isotopomers LiD and LiT. In these cases the phase is staying stationary for longer times, figure 7(b), providing strong isotope effect in the population dynamics.

5. Concluding remarks

The ground and lowest excited state potentials of molecules are typically isolated. For higher energies even for simple

molecules there is a forest of excited states interacting by non Born–Oppenheimer terms. This is the regime we discuss here. During an ultrafast excitation a set of such electronically excited states is coherently accessed. Therefore the nonadiabatic transition is often an exchange of amplitude between states that are both populated already before the exchange. It is the extent of this exchange that is different for different isotopomers.

The exact equations of motion show that the transient rate of exchange between two states is driven by the coherence between them, e.g., equation (9). The coherence between any two wave packets is determined by the motion of the nuclei on the two potentials and the resulting interference. The mass effect on the rate arises in two ways. There is the classical effect that heavier molecules transverse the coupling region more slowly. There is the quantum mechanical effect expressed through the overlap integral of the two wave packets. The net transfer is roughly the rate times the duration and the duration is longer for heavier molecules. This makes the dependence on the mass nonlinear. But at early times a Gaussian parameterization, equation (6), is suitable and this allows us to identify the main factors that play a role in the magnitude of the isotope effect.

Acknowledgments

This work was supported by the AMOS program within the Chemical Sciences, Geosciences and Biosciences Division of the Office of Basic Energy Sciences, Office of Science, US Department of Energy, Award DE-SC0012628 and by the Horizon2020 FET open project COPAC 766563. F R acknowledges support from the Fonds National de la Recherche Scientifique, Belgium (F R S-FNRS, PDR T.0132.16, J.0012.18). S V D W acknowledges the support of a Ph.D. fellowship from F R S-FNRS. Computational resources have been provided by the Consortium des Equipments de Calcul Intensif (CECI), funded by the F R S-FNRS under Grant No. 2.5020.11.

ORCID iDs

Ksenia G Komarova https://orcid.org/0000-0001-6603-1377
Françoise Remacle https://orcid.org/0000-0001-7434-5245

References

[1] Galbraith M C E, Scheit S, Golubev N V, Reitsma G, Zhavoronkov N, Despré V, Lépine F, Kuleff A I, Vrakking M J J, Kornilov O, Köppel H and Mikosch J 2017 Few-femtosecond passage of conical intersections in the benzene cation *Nat. Commun.* **8** 1018
[2] Nisoli M, Decleva P, Calegari F, Palacios A and Martín F 2017 Attosecond electron dynamics in molecules *Chem. Rev.* **117** 10760–825
[3] Ramasesha K, Leone S R and Neumark D M 2016 Real-time probing of electron dynamics using attosecond time-resolved spectroscopy *Annu. Rev. Phys. Chem.* **67** 41–63
[4] Medišauskas L, Patchkovskii S, Harvey A, Brambila D S, Neidel C, Klei J, Rouzée A, Vrakking M J J and Ivanov M Y 2015 Initial electronic coherence in molecular dissociation induced by an attosecond pulse *Phys. Rev.* A **92** 053403
[5] Vrakking M J J and Lepine F 2019 *Attosecond Molecular Dynamics* (Cambridge: The Royal Society of Chemistry) p 500
[6] Bennett K, Kowalewski M and Mukamel S 2016 Nonadiabatic dynamics may be probed through electronic coherence in time-resolved photoelectron spectroscopy *J. Chem. Theor. Comput.* **12** 740–52
[7] Neville S P, Averbukh V, Patchkovskii S, Ruberti M, Yun R, Chergui M, Stolow A and Schuurman M S 2016 Beyond structure: ultrafast x-ray absorption spectroscopy as a probe of non-adiabatic wavepacket dynamics *Faraday Discuss.* **194** 117–45
[8] Wu G R, Neville S P, Schalk O, Sekikawa T, Ashfold M N R, Worth G A and Stolow A 2016 Excited state non-adiabatic dynamics of N-methylpyrrole: a time-resolved photoelectron spectroscopy and quantum dynamics study *J. Chem. Phys.* **144** 014309
[9] Neville S P, Wang Y, Boguslavskiy A E, Stolow A and Schuurman M S 2016 Substituent effects on dynamics at conical intersections: allene and methyl allenes *J. Chem. Phys.* **144** 014305
[10] Cao W, Warrick E R, Fidler A, Leone S R and Neumark D M 2018 Excited-state vibronic wave-packet dynamics in H2 probed by XUV transient four-wave mixing *Phys. Rev.* A **97** 023401
[11] Peters W K, Couch D E, Mignolet B, Shi X, Nguyen Q L, Fortenberry R C, Schlegel H B, Remacle F, Kapteyn H C, Murnane M M and Li W 2017 Ultrafast 25 fs relaxation in highly excited states of methyl azide mediated by strong nonadiabatic coupling *Proc. Natl Acad. Sci. USA* **114** E11072–81
[12] Okino T, Furukawa Y, Nabekawa Y, Miyabe S, Amani Eilanlou A, Takahashi E J, Yamanouchi K and Midorikawa K 2015 Direct observation of an attosecond electron wave packet in a nitrogen molecule *Sci. Adv.* **1** e1500356
[13] Wolter B, Pullen M G, Le A-T, Baudisch M, Doblhoff-Dier K, Senftleben A, Hemmer M, Schröter C D, Ullrich J, Pfeifer T, Moshammer R, Gräfe S, Vendrell O, Lin C D and Biegert J 2016 Ultrafast electron diffraction imaging of bond breaking in di-ionized acetylene *Science* **354** 308–12
[14] Baer M 2006 *Beyond Born–Oppenheimer: Electronic Nonadiabatic Coupling Terms and Conical Intersections* (New York: Wiley) pp 28–43
[15] Zewail A H 1994 *Femtochemistry: Ultrafast Dynamics of the Chemical Bond* (Singapore: World Scientific) p 604
[16] Nest M, Remacle F and Levine R D 2008 Pump and probe ultrafast electron dynamics in LiH: a computational study *New J. Phys.* **10** 025019–24
[17] Spelsberg D and Meyer W 2001 Dipole-allowed excited states of N_2: potential energy curves, vibrational analysis, and absorption intensities *J. Chem. Phys.* **115** 6438–49
[18] Levine R D 2017 Photochemistry of highly excited states *Proc. Natl Acad. Sci. USA* **114** 13594–6
[19] Ajay J S, Komarova K G, Remacle F and Levine R D 2018 Time-dependent view of an isotope effect in electron–nuclear nonequilibrium dynamics with applications to N_2 *Proc. Natl Acad. Sci. USA* **115** 5890–5
[20] Granucci G and Persico M 1995 Coherent excitation of wavepackets in two electronic states. Interference effects at an avoided crossing *Chem. Phys. Lett.* **246** 228–34
[21] Ben-Nun M and Levine R D 1995 Short-time dynamics on several electronic states: formalism and computational study of I2 in rare gas solvents *Chem. Phys.* **201** 163–87
[22] Palacios A, Feist J, González-Castrillo A, Sanz-Vicario J L and Martín F 2013 Autoionization of molecular hydrogen: where do the Fano lineshapes go? *Chem. Phys. Chem.* **14** 1456–63

[23] Wildenberg S V D, Mignolet B, Levine R D and Remacle F 2019 Temporal and spatially resolved imaging of the correlated nuclear–electronic dynamics and of the ionized photoelectron in a coherently electronically highly excited vibrating LiH molecule *J. Chem. Phys.* **151** 134310
[24] Gadea F X and Leininger T 2006 Accurate *ab initio* calculations for LiH and its ions, LiH^+ and LiH^- *Theor. Chem. Acc.* **116** 566–75
[25] Holka F, Szalay P G, Fremont J, Rey M, Peterson K A and Tyuterev V G 2011 Accurate *ab initio* determination of the adiabatic potential energy function and the Born–Oppenheimer breakdown corrections for the electronic ground state of LiH isotopologues *J. Chem. Phys.* **134** 094306
[26] Arasaki Y and Takatsuka K 2013 Pulse-train photoelectron spectroscopy of electronic and nuclear dynamics in molecules *ChemPhysChem* **14** 1387–96
[27] Sato T and Ishikawa K L 2013 Time-dependent complete-active-space self-consistent-field method for multielectron dynamics in intense laser fields *Phys. Rev.* A **88** 023402
[28] Levine R D and Bernstein R B 1974 *Molecular Reaction Dynamics* (New York: Oxford University Press) pp 176–9
[29] Zener C 1932 Non-adiabatic crossing of energy levels *Proc. R. Soc.* A **137** 696–702
[30] Heller E J 1975 Time-dependent approach to semiclassical dynamics *J. Chem. Phys.* **62** 1544–55
[31] Kubo R 1962 Generalized cumulant expansion method *J. Phys. Soc. Jpn.* **17** 1100–20
[32] Komarova K G, Remacle F and Levine R D 2019 Time resolved mechanism of the isotope selectivity in the ultrafast light induced dissociation in N_2 *J. Chem. Phys.* **151** 114308
[33] Smith F T 1969 Diabatic and adiabatic representations for atomic collision problems *Phys. Rev.* **179** 111–23
[34] Ajay J S, Komarova K G, Van Den Wildenberg S, Remacle F and Levine R D 2018 *Attophotochemistry: Coherent Electronic Dynamics and Nuclear Motion* (London: The Royal Society of Chemistry) ch 9 pp 308–47
[35] Remacle F, Nest M and Levine R D 2007 Laser steered ultrafast quantum dynamics of electrons in LiH *Phys. Rev. Lett.* **99** 183902
[36] Ghafur O, Rouzee A, Gijsbertsen A, Siu W K, Stolte S and Vrakking M J J 2009 Impulsive orientation and alignment of quantum-state-selected NO molecules *Nat. Phys.* **5** 289–93
[37] Fleischer S, Khodorkovsky Y, Gershnabel E, Prior Y and Averbukh I S 2012 Molecular alignment induced by ultrashort laser pulses and its impact on molecular motion *Isr. J. Chem.* **52** 414–37
[38] Knowles P J and Werner H J 1985 An efficient second-order MC SCF method for long configuration expansions *Chem. Phys. Lett.* **115** 259–67
[39] Werner H J and Knowles P J 1985 A second order multiconfiguration SCF procedure with optimum convergence *J. Chem. Phys.* **82** 5053–63
[40] Simah D, Hartke B and Werner H-J 1999 Photodissociation dynamics of H2S on new coupled *ab initio* potential energy surfaces *J. Chem. Phys.* **111** 4523–34
[41] Werner H J and Meyer W 1981 MCSCF study of the avoided curve crossing of the two lowest $1\Sigma+$ states of LiF *J. Chem. Phys.* **74** 5802–7
[42] Werner H-J *et al* 2015 MOLPRO, a package of *ab initio* programs http://molpro.net
[43] Kosloff R 1988 Time-dependent quantum-mechanical methods for molecular dynamics *J. Phys. Chem.* **92** 2087–100
[44] Frigo M and Johnson S G 2005 The design and implementation of FFTW3 *Proc. IEEE* **93** 216–31